

# A Model of Gas-Phase Transport During the Initial Stages of Sintering of Silicon Carbide

Anil Kaza, M. John Matthewson,<sup>†</sup> Dale Niesz, Richard L. Haber, and Mark A. Rossi

Department of Materials Science and Engineering, Rutgers, The State University of New Jersey, Piscataway, New Jersey 08854

Carbon, which is often used as an additive to silicon carbide powder, is thought to facilitate densification during sintering by aiding the removal of the native SiO<sub>2</sub> layer, which is present on the starting SiC powder. The mechanism is the reduction of SiO<sub>2</sub> to SiC with the formation of primarily CO gas, which diffuses out from the porous compact at a temperature below the normal sintering temperature. It has been found beneficial to hold the compact at an intermediate temperature to allow time for the CO and other gases to diffuse out before the pores close. We investigate this process using a computational model based on codiffusion of multiple gas species, which enables prediction of the gas and condensed phase compositions as a function of time and position in the specimen. The results are used to determine the optimum holding time for complete SiO<sub>2</sub> removal as a function of key parameters, such as specimen thickness, particle size, temperature, etc., as well as the necessary amount of C additive. The results of the modeling are consistent with the experimentally observed spatial variation of density and composition in SiC compacts.

## I. Introduction

THE successful pressureless sintering of silicon carbide (SiC) was first discovered by Prochazka in 1977,<sup>1</sup> using boron and carbon as sintering additives. Rijswijk and Shanefield<sup>2</sup> suggested that the presence of C increases the silicon vacancy concentration and increases the effective diffusion rate of SiC. However, it is widely believed that the addition of C aids the removal of the native surface layer of SiO<sub>2</sub> on the SiC particles.<sup>3–6</sup> It is thought that one of the factors leading to high-density SiC is the complete removal of the oxide layer at temperatures much lower than typical sintering temperatures. Ness and Rafaniello<sup>7</sup> showed that holding the powder compact in a vacuum for some time, at an intermediate temperature in the range of 1400°–1700°C before heating to the sintering temperature, resulted in higher final density. They also observed density gradients in the sintered SiC, with higher densities near the surfaces. They suggested that the high densities were most likely due to the faster rate of removal of CO near the surfaces, which enabled the reaction between C and SiO<sub>2</sub> to proceed faster.

In practice, the amount of C added to the starting SiC powder is determined experimentally. The optimum amount of C is important because if the C content is low, the SiO<sub>2</sub> reduction will be incomplete leading to low final densities, and if the C content is too high, the resultant C inclusions will lead to deterioration of mechanical properties.<sup>8</sup> The holding time at a particular temperature is also critical—not all SiO<sub>2</sub> will be removed with a shorter holding time, while a prolonged hold leads to grain coarsening and to a less efficient heating cycle.<sup>9</sup>

F. Wakai—contributing editor

This paper describes a computational model that tracks diffusion of multiple gas species and so predicts the evolution of the composition of the gas and condensed phases as a function of time and position. The results are used to examine how final composition varies with hold time and in particular, examines the needed hold time for complete removal of SiO<sub>2</sub>.

## II. The Model

### (1) Gas-Phase Diffusion Modeling

We describe a computational model that is used to predict the removal rate of SiO<sub>2</sub> during sintering/hot-pressing of SiC. The model considers the diffusion of multiple gas species through the porous SiC compact, coupled to the creation of more gas as the reactions with the condensed species progress.

The so-called dusty-gas model (DGM) is used to describe the transport of multiple gas species through a porous body by treating the solid particles as massive and effectively stationary gas molecules. The particular implementation of the DGM used here is due to Mason and Malinauskas<sup>10</sup> and incorporates three transport mechanisms, namely Knudsen diffusion, continuum or interdiffusion, and viscous flow. Knudsen diffusion is important when the pore sizes are small enough that the gas molecule–pore wall interactions dominate over the interactions between the gas molecules, i.e. when the mean free path is long compared with the shortest dimension of the containing pores. The interdiffusion accounts for the interaction between the multiple gas species (different species diffuse at different rates), while the diffusion due to viscous flow arises from pressure gradients in the gas mixture.

Mason and Malinauskas<sup>10</sup> also integrate surface diffusion into their DGM—we ignore this mechanism, firstly because typical SiC compacts have a small specific surface area that tends to favor the other three mechanisms and secondly for the pragmatic reason that little or no information is available on the relevant parameters. In contrast, the three mechanisms that are modeled here depend entirely on gas properties that are well-known and characterized.

The DGM diffusion equation for the *i*th gas species in a mixture of gases consisting of *v* species is given by<sup>10</sup>

$$\sum_{j=1}^v \frac{p_j}{p D_{ij}} \left( \frac{J_i}{n_i} - \frac{J_j}{n_j} \right) + \frac{1 - \Delta_{id}}{D_{ik}} \left[ \frac{J_i}{n_i} + \frac{B_0}{\eta} \nabla p \right] = - \left( \frac{\nabla p_i}{p_i} \right) \quad (1)$$

where  $J_i$ ,  $n_i$ , and  $p_i$  are the flux, number of moles per unit volume, and partial pressure of the *i*th species and  $p$  is the total pressure. The gases are assumed to be ideal, so that

$$p_i = n_i RT \quad (2)$$

where  $R$  is the gas constant and  $T$  is the absolute temperature.  $D_{ij}$  is the interdiffusion coefficient between the *i*th and *j*th species

Manuscript No. 26092. Received March 31, 2009; approved June 2, 2009.

<sup>†</sup>Author to whom correspondence should be addressed. e-mail: mjohnm@fracture.rutgers.edu

and is given by<sup>10</sup>

$$D_{ij} = \frac{3}{8} \left( \frac{\pi k_B T}{2\mu_{ij}} \right)^{1/2} \frac{1}{n N_A \pi \sigma_{ij}^2} \quad (3)$$

Here  $k_B$  is the Boltzmann constant,  $N_A$  is Avogadro's number,  $n$  is total number of moles per unit volume,

$$\mu_{ij} = m_i m_j / (m_i + m_j) \quad (4)$$

is the reduced mass of the  $ij$  molecule pair and

$$\sigma_{ij} = (\sigma_i + \sigma_j) / 2 \quad (5)$$

is the average of the hard sphere diameters of the  $ij$  molecule pair. This expression for  $D_{ij}$  is the first order approximation described by Mason and Malinauskas<sup>10</sup>; it ignores the dependence of  $D_{ij}$  on composition and of  $\sigma_{ij}$  on temperature, both of which are small effects.  $D_{iK}$  is the Knudsen diffusion coefficient given by

$$D_{iK} = \frac{4}{3} \left( \frac{8k_B T}{\pi m_i} \right)^{1/2} K_0 \quad (6)$$

where the value of  $K_0$  depends only on the pore geometry and the gas-surface scattering law.  $K_0$  has been defined for simple geometries; in this work

$$K_0 = r/2 \quad (7)$$

is used, which is appropriate for a long, straight, circular tube of radius  $r$  with diffuse scattering.

The rate of both interdiffusion and Knudsen diffusion is controlled by the pore structure (open porosity assumed in this work) and thus porosity ( $\epsilon$ ) and tortuosity ( $q$ ) of a given porous medium. An effective diffusion coefficient can be calculated based on a ideal diffusion coefficient that is attenuated by a porosity/tortuosity factor of the form  $\epsilon/q$ .<sup>10</sup> Specifically

$$D_{ij,\text{eff}} = \left( \frac{\epsilon}{q} \right) D_{ij} \text{ and } D_{iK,\text{eff}} = \left( \frac{\epsilon}{q} \right) D_{iK} \quad (8)$$

$B_0$  in Eq. (1) also depends on the pore geometry and is given by

$$B_0 = \left( \frac{\epsilon}{q} \right) \frac{r^2}{8} \quad (9)$$

for pores that are straight, circular tubes of radius  $r$ .<sup>10</sup>

Hirschfelder *et al.*<sup>11</sup> describe a detailed model for the viscosity of a gas mixture. In the present work, it is found that the pressure of CO is about two orders of magnitude higher than any other species in the temperature range of interest. CO therefore dominates and so, to a good approximation, the viscosity of the mixture is taken as the same as the viscosity of pure CO. Hirschfelder and colleagues give the following relationship for the viscosity of an ideal gas:

$$\eta = \frac{5}{16\pi\sigma^2\Omega^{(2,2)}} \left( \frac{\pi M k_B T}{N_A} \right)^{1/2} \quad (10)$$

where  $M$  is the molecular weight and  $\sigma$  is the hard sphere radius;  $\Omega^{(2,2)}$  corrects for the dependence of  $\sigma$  on temperature and Hirschfelder and colleagues give expressions and tabulated values from which  $\Omega^{(2,2)}$  is determined. In our case its value is close to unity.

## (2) Solution of the DGM Equation

Equation (1) is solved using a finite difference algorithm. In this work, we restrict the discussion to a one-dimensional problem, i.e. the body is assumed to be an infinite flat plate. The body is broken up into a number of discrete nodes (typically 101) but using more or fewer nodes has a negligible impact on the results. The pressure gradient between adjacent nodes is approximated by the finite difference equation

$$\nabla p = \frac{dp}{dx} \approx \frac{p_{k+1} - p_k}{\delta x} \quad (11)$$

where  $p_k$  and  $p_{k+1}$  are the pressures at nodes  $k$  and  $k+1$ , and  $\delta x$  is the distance between the nodes. In addition to spatial discretization, the problem is solved by taking small time steps of size  $\delta t$ . The fluxes of the various gas species are strongly coupled in Eq. (1). To effectively uncouple them and simplify the calculations, the flux of the  $i$ th species at any time,  $J_i$  in Eq. (1), is calculated from the fluxes of all the other species ( $J_j$  for  $j \neq i$ ) calculated in the previous time step. Because the time steps are small, the change in flux between each step is negligible, so this approximation does not introduce significant error, but does considerably increase computational efficiency. This assumption is verified by the observation that the results are insensitive to large changes in the size of the time steps.

Figure 1 shows several gas species in equilibrium with the starting composition of SiC, C, and SiO<sub>2</sub>, as a function of temperature. Many species have an extremely small partial pressure in the temperature range of interest ( $\sim 1200$ – $2500$  K) thus having a negligible impact on the rate of mass transfer in the gas phase, and so can be safely ignored in the modeling.

The model considers the diffusion of four gas species through the specimen pores. These include CO, the most abundant gas; SiO, the most abundant gas containing Si (SiO is thought to control the rate of interparticle neck growth),<sup>12</sup> and CO<sub>2</sub>. O<sub>2</sub> is also considered, even though other species are more abundant, firstly, because it is a convenient vehicle for the calculations, and secondly, it is a direct measure of oxygen activity.

The calculations require a few species-specific constants. Equation (2) requires a molecular hard sphere diameter for each species and Eq. (10) requires a collision diameter for CO. Table I lists the values used in this work and their sources.

The equilibrium partial pressures of the gas species present in the specimen pores can be determined if both the temperature

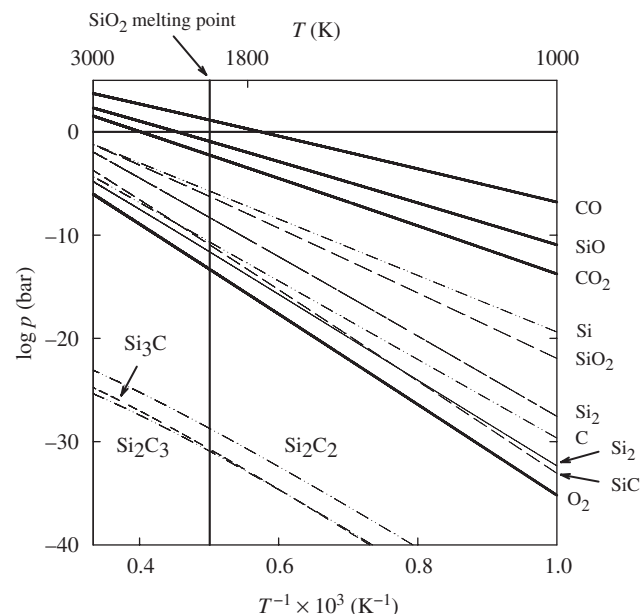


Fig. 1. Gas pressures as a function of temperature for several species in equilibrium with solid SiC, C and solid ( $T < 1996$  K) or liquid ( $T > 1996$  K) SiO<sub>2</sub>.

**Table I. Molecular Diameters for the Various Gas Species**

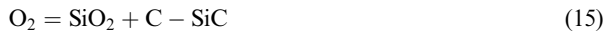
Parameter	Value (nm)	References
CO diameter, $d_{\text{CO}}$	0.38	Kaye and Laby <sup>13</sup>
$d_{\text{CO}_2}$	0.45	Kaye and Laby <sup>13</sup>
$d_{\text{O}_2}$	0.35	Kaye and Laby <sup>13</sup>
$d_{\text{SiO}}$	0.36	Kang and Kunc <sup>14</sup>
Collision diameter, $\sigma_{\text{CO}}$	0.37	Hirschfelder <i>et al.</i> <sup>11</sup>

and the nature of the condensed species are known. Several thermodynamic systems can be identified depending on which solid species are present. The three most important here are: Regime 1, where SiC, C, and SiO<sub>2</sub> are all present. In Regime 2, SiC and C are present, which occurs after the SiO<sub>2</sub> is depleted. If insufficient carbon is present, it can become depleted instead of SiO<sub>2</sub>, giving Regime 3, where only SiC and SiO<sub>2</sub> are present. In the current work, we can ensure that sufficient carbon is always present for complete SiO<sub>2</sub> removal, so that only the first two regimes are considered here.

### (3) Thermodynamics

The computational model calculates the equilibrium conditions at each node using the regime operative at that node at that time. A more general algorithm for determining the position of equilibrium, which does not make assumptions about the regime, could be used for determining the equilibrium gas pressures, but it would be significantly less computationally efficient. Treating the small number of regimes individually does add some complexity to the computer program, but results in much faster execution than a general free energy minimization approach.

(A) *Regime 1:* In Regime 1, the determination of equilibrium gas partial pressures can be performed simply and directly because there are three condensed phases and three atomic species. As a result, any gas species can be expressed in terms of the condensed species alone



The standard free energy change for each of the above reactions is determined by summing the free energies of the individual species. For example, for CO, Eq. (12) gives

$$\Delta G_{\text{CO}}^\circ = 0.5G_{\text{SiO}_2}^\circ + 1.5G_{\text{C}}^\circ - 0.5G_{\text{SiC}}^\circ - G_{\text{CO}}^\circ \quad (16)$$

The free energy of the  $i$ th species is given by

$$G_i = G_i^\circ - H_{\text{SER},i}^\circ \quad (17)$$

where  $G_i^\circ$  and  $H_{\text{SER},i}^\circ$  are the standard free energy and standard enthalpic reference, i.e. the enthalpy of the constituent elements of species  $i$  at 298 K. Values of  $G^\circ - H_{\text{SER}}^\circ$  for the various species have been calculated from the semiempirical equation

$$G^\circ - H_{\text{SER}}^\circ = c_1 + c_2T + c_3T \ln T + c_4T^2 + c_5/T + c_6T^3 + c_8T^{1/2} \quad (18)$$

Values for the coefficients  $c_i$  ( $i = 1 \dots 8$ ) have been obtained from the TAPP program<sup>15</sup> that derives these coefficients from data in the JANAF tables.<sup>16,17</sup> The results compare favorably with the more recent NIST thermodynamic data.<sup>18</sup>

The equilibrium constant can be calculated and expressed in terms of the activities. For CO

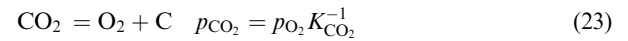
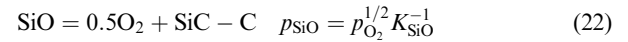
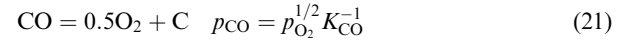
$$K_{\text{CO}} = \exp\left(-\frac{\Delta G_i^\circ}{RT}\right) = \frac{a_{\text{SiO}_2}^{0.5} a_{\text{C}}^{1.5} a_{\text{SiC}}^{-0.5}}{p_{\text{CO}}} \quad (19)$$

Here the partial pressure of CO is a surrogate for its activity and so has units of atmospheres (1 atm being the standard state for the thermodynamic data). Because we are assuming all condensed species are at or near to their standard state, their activities are unity. This gives  $p_{\text{CO}}$  directly

$$p_{\text{CO}} = \exp\left(\frac{\Delta G_i^\circ}{RT}\right) \quad (20)$$

The partial pressures of the other gas species are calculated in an analogous fashion.

(B) *Regime 2:* In Regime 2, the calculation of equilibrium gas partial pressures cannot be performed explicitly because oxygen is absent from the condensed phases. As a result, the various gas species cannot be expressed in terms of the condensed species alone. However, they can be expressed in terms of the condensed species and any oxygen containing gas; O<sub>2</sub> has been used for this case



The additional constraint needed to solve these simultaneous equations is mass balance; namely that the quantity of each atomic species does not change as the system moves to equilibrium. For this regime, it is sufficient to only consider oxygen. The total number of moles of oxygen atoms (i.e. g-atoms of oxygen) is given by

$$n_{\text{O}} = A(p_{\text{CO}} + p_{\text{SiO}} + 2p_{\text{CO}_2} + 2p_{\text{O}_2}) \quad (24)$$

where  $A$  is a factor that converts from gas partial pressure (in atmospheres) to number of moles, taking into account the properties of an ideal gas, the volume associated with the node under consideration, and the porosity. Substituting in terms of  $p_{\text{O}_2}$  from Eqs. (21) to (23), gives

$$n_{\text{O}} = A\left(p_{\text{O}_2}^{1/2} K_{\text{CO}}^{-1} + p_{\text{O}_2}^{1/2} K_{\text{SiO}}^{-1} + 2p_{\text{O}_2} K_{\text{CO}_2}^{-1} + 2p_{\text{O}_2}\right) \quad (25)$$

Noting that  $n_{\text{O}}$  is a known constant, because it is the total amount of oxygen at the node at the start of the equilibration step, Eq. (25) is a quadratic in  $p_{\text{O}_2}^{1/2}$ , which can be readily solved using standard methods.

### (4) Diffusion and Reequilibration

The calculation of diffusion and reequilibration at each time step and at each node involves three stages. Firstly, diffusion of the gases in, or out of each node is quantified. This changes the partial pressures, so that the gases are no longer in equilibrium with the condensed phases. Secondly, the position of equilibrium is calculated using the methods described above, accounting for any change in the temperature at the node due to a heating cycle, or thermal conductivity. Thirdly, mass balance is used to update the composition of the solid phase that results after putting the system back into equilibrium. We assume that the reaction kinetics are fast compared with the diffusion at each node, which is reasonable at high temperature. Further, if reaction kinetics were rate determining, the experimentally observed

density gradients<sup>7</sup> would not be seen. If reaction kinetics were important, and if rate constants were available, the third step would involve moving the system back toward equilibrium by an amount proportional to how far it is away from equilibrium.

For sufficiently thick green bodies, the gas flow kinetics must be rate controlling and the assumption of fast reaction kinetics and hence the assumption of local equilibrium is justified. Because density gradients are observed in bodies on the order of 1 cm in thickness,<sup>7</sup> this suggests that “sufficiently thick” is around 1 cm or perhaps even less.

In more detail, the following calculations are made for any given gas species. The partial pressure of the species under consideration at the start of a time step and at node  $k$  is given by  $p_k$  and is the equilibrium partial pressure returned at the end of the previous time step. The DGM is used to calculate the change in the number of moles of the gas caused by diffusion. From this, the partial pressure at the end of the diffusion step,  $p_k^{\text{diff}}$ , is calculated using

$$p_k^{\text{diff}} = p_k - RT \left( \frac{\delta t}{\delta x} \right) \frac{(J_{k+1} - J_k)}{\varepsilon_k} \quad (26)$$

where  $J_k$  is the flux between the nodes  $k-1$  and  $k$ , and  $\varepsilon_k$  is the porosity at node  $k$ .

After recalculation of the equilibrium partial pressure  $p_k^{\text{eq}}$ , (which need not be the same as  $p_k$  because the temperature during the previous time step might be different) the system is returned to equilibrium because we are modeling the case where each node remains in local equilibrium because the gas diffusion is rate limiting. The gas pressure is therefore adjusted from  $p_k^{\text{diff}}$  to  $p_k^{\text{eq}}$ , which involves adding or subtracting matter from the condensed phases.

The change in the quantity of each condensed species is calculated using the reactions given in Eqs. (12)–(15). For example, in Regime 1, the change in the number of moles of each solid is given by

$$\delta n_C = -1.5\delta n_{\text{CO}} + 0.5\delta n_{\text{SiO}_2} - 2\delta n_{\text{CO}_2} - \delta n_{\text{O}_2} \quad (27)$$

$$\delta n_{\text{SiC}} = 0.5\delta n_{\text{CO}} - 0.5\delta n_{\text{SiO}_2} + \delta n_{\text{CO}_2} + \delta n_{\text{O}_2} \quad (28)$$

$$\delta n_{\text{SiO}_2} = -0.5\delta n_{\text{CO}} - 0.5\delta n_{\text{SiO}_2} - \delta n_{\text{CO}_2} + \delta n_{\text{O}_2} \quad (29)$$

The coefficients in each equation are the stoichiometric coefficients for the corresponding solid in Eqs. (12)–(15) with the sign changed to recognize that if the stoichiometric coefficient is positive, that amount of solid decreases when the amount of gas increases. Similar results can be obtained for Regime 2 using Eqs. (21)–(23)

$$\delta n_C = -\delta n_{\text{CO}} + \delta n_{\text{SiO}_2} - \delta n_{\text{CO}_2} \quad (30)$$

$$\delta n_{\text{SiC}} = -\delta n_{\text{SiO}_2} \quad (31)$$

At the end of each time step, it is possible that the conditions at any given node have caused a change in regime. For example, for a node initially in Regime 1, the  $\text{SiO}_2$  may become depleted and the number of moles of  $\text{SiO}_2$  will be negative after adjustment of the quantities described above, when the system is moved back to equilibrium. Because the time step is small, the negative quantities are extremely small and do not affect the accuracy of the model. However, at the start of the next time step, the zero or negative quantity of  $\text{SiO}_2$  means that the node has changed to Regime 2 and calculation methods are adjusted accordingly.

Another possibility is that a previously absent solid phase could be deposited during the time step. In this study, it would correspond to deposition of  $\text{SiO}_2$  at a node that is currently in Regime 2, so that it reverses to Regime 1. While this does not occur in any of the cases described here, it can be important under other conditions, such as when the starting composition is not uniform and includes regions deficient in C. The effect of

nonuniform composition will be described in a later paper. However, even though no regime reversal occurs in this work, the program code to detect this situation has been used. It involves detecting when the chemical activity of any absent solid phase exceeds unity—in this case the system would lower its free energy by forming that absent phase so changing the regime.

### III. The “Reference” Conditions

While we have studied the effect of changing a variety of parameters on the behavior of the system, a single set of parameters has been used to provide a “reference” case. They are shown in Table II and are in the range typical of values encountered when sintering SiC parts.<sup>7,19</sup>

The model describes multispecies gas transport through narrow channels connecting pores. As described previously, these channels can be likened to narrow cylindrical tubes. The Knudsen number ( $K_n$ ) is the ratio of the mean free path of the gas molecules ( $\lambda$ ) and the smallest physical dimension of the gas path (the pore diameter,  $2r_{\text{pore}} = 32$  nm, in the standard case). Its value determines the predominant type of diffusion. Because CO is the dominant gas species

$$\lambda_{\text{CO}} = \frac{k_B T}{\sqrt{2} \pi p_{\text{CO}} \sigma_{\text{CO}}} \quad (32)$$

A CO pressure of 0.28 atm and standard conditions described by parameters tabulated in Tables I and II results in a mean free path of 1.23  $\mu\text{m}$ . Therefore, for CO, the  $K_n$  is 39.3; showing that free molecular transport is dominant.

Figures 2 and 3 show how the partial pressures of the CO varies in both time and position for a large flat plate under the reference conditions given in Table II. The surrounding environment is assumed to be a vacuum, which optimizes the rate of CO removal. Initially, all gases are at the equilibrium partial pressure for an isothermal temperature of 1640 K. There is no driving force for diffusion except at the surface. As time progresses, the gasses diffuse out from beneath the surface, gradually exhausting the  $\text{SiO}_2$ . A reaction front therefore propagates into the body corresponding to the front, where the system is changing from Regime 1 to Regime 2. Because the interior of the specimen is in Regime 1, the partial pressures do not change with time, so there is negligible driving force for diffusion until the reaction front arrives, explaining the flat-topped pressure profiles. Because CO is the dominant gas species, it controls diffusion kinetics. Even though the DGM is non-Fickian, in that the effective diffusion coefficient for each species is not independent of the pressure, it is roughly so. Also, the volume of CO evolved from each node is much larger than the volume of the pores at the node. Therefore, the reaction front moves slowly and approximately quasi-static conditions for the diffusion are established. Therefore, the pressure profile for CO while in Regime 2 is approximately that for quasi-static Fickian diffusion in one dimension, namely the pressure decreases linearly from the equilibrium pressure at the reaction front to zero at the surface. The partial pressures of the other gas species are primarily controlled by CO, due to its abundance. Therefore, their pressure profiles are controlled by the constraint of equilibrium rather than by the rate of diffusion. The equilibrium between these and CO can be examined using the following reactions, noting that

**Table II. Parameter Values Used for the Reference Simulation**

Specimen thickness ( $l$ )	10 mm
Pore radius ( $r$ )	16 nm
Porosity ( $\varepsilon$ )	0.4
Tortuosity ( $q$ )	5
Mole fraction of carbon ( $X_C$ )	3.3%
Mole fraction of $\text{SiO}_2$ ( $X_{\text{SiO}_2}$ )	1%
Temperature ( $T$ )	1640 K
External environment	Vacuum

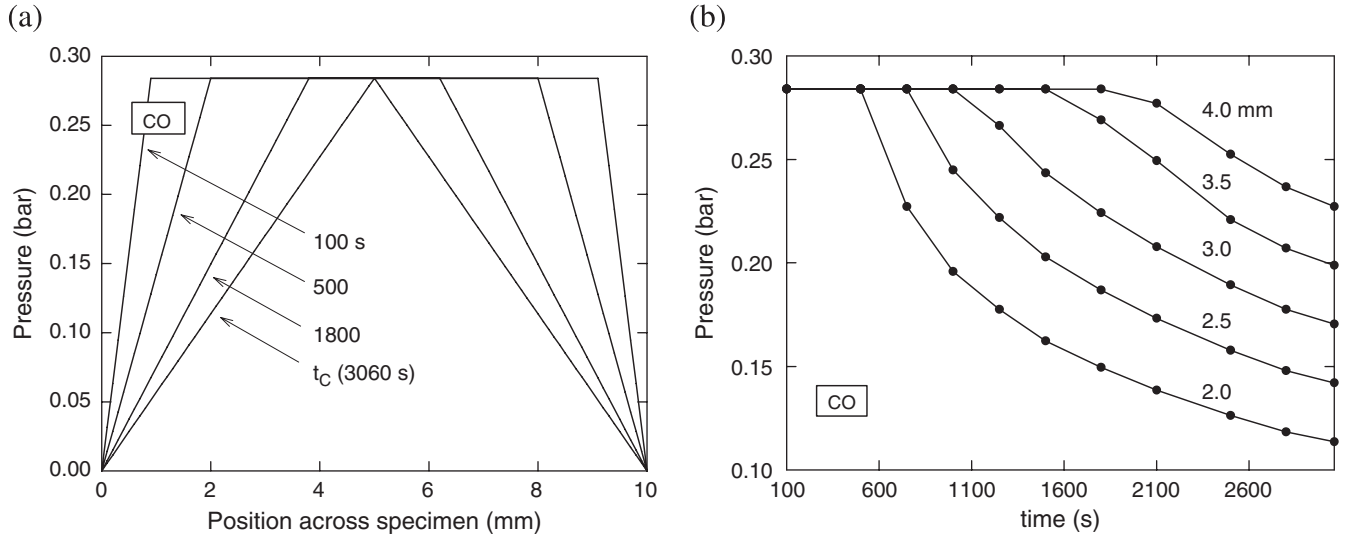


Fig. 2. Partial pressure of CO (a) as a function of position at several times and (b) as a function of time at several positions beneath the specimen surface.

only SiC and C are present in the solid phase in Regime 2:

$$\left. \begin{aligned} \text{SiO} = \text{CO} - \text{SiC} &\Rightarrow p_{\text{SiO}} \sim p_{\text{CO}} \\ \text{CO}_2 = 2\text{CO} - \text{C} &\Rightarrow p_{\text{CO}_2} \sim p_{\text{CO}}^2 \\ \text{O}_2 = 2\text{CO} - 2\text{C} &\Rightarrow p_{\text{O}_2} \sim p_{\text{CO}}^2 \end{aligned} \right\} \quad (33)$$

This explains why, for a linear CO profile, the SiO profile is also linear while the O<sub>2</sub> and CO<sub>2</sub> profiles are parabolic (Fig. 3).

Figure 4 shows how the concentration of C and SiO<sub>2</sub> vary in position across the specimen thickness at various times, including the time for complete removal of SiO<sub>2</sub>.

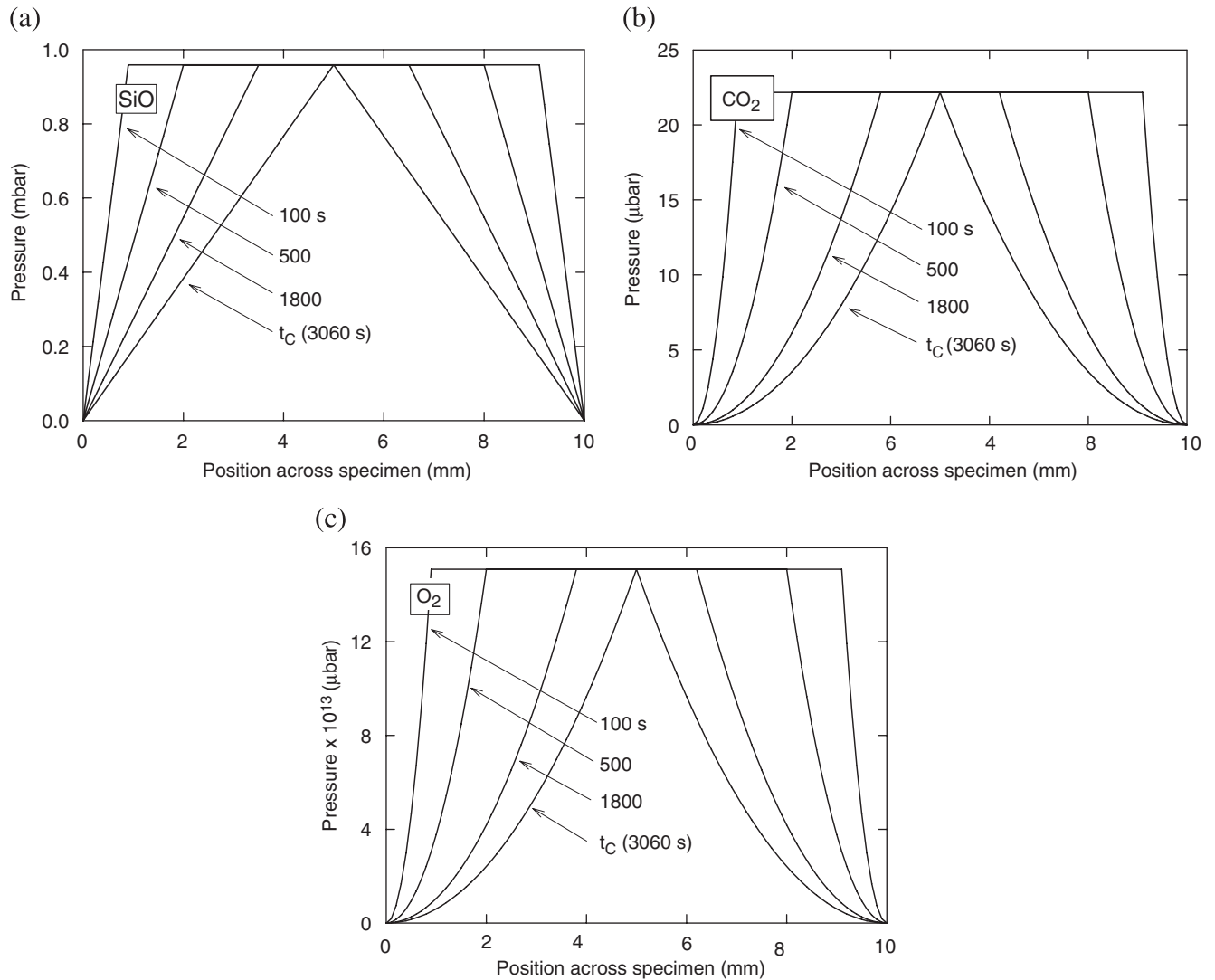


Fig. 3. Partial pressure profiles of (a) SiO, (b) CO<sub>2</sub>, and (c) O<sub>2</sub> as a function of position across the sample thickness at various times.

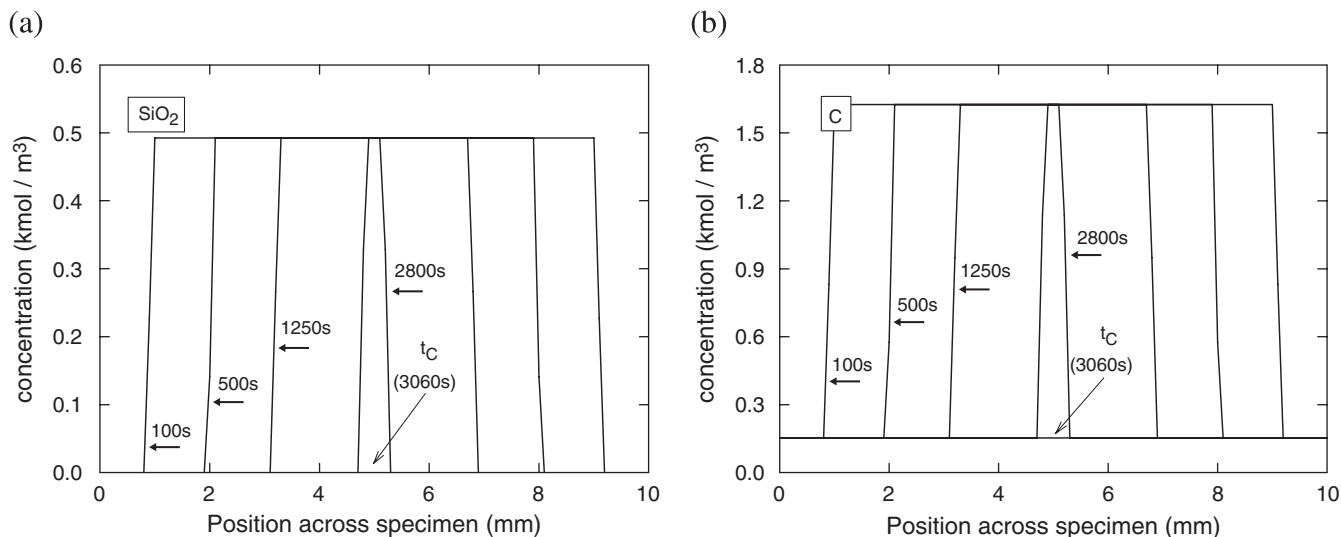


Fig. 4. Profiles of (a)  $\text{SiO}_2$  and (b) C as a function of position at various times during the temperature hold.

It can be seen that  $\text{SiO}_2$  is exhausted first at the nodes at the surface and last at the center node. An abrupt interface is seen separating the nodes where  $\text{SiO}_2$  is exhausted, from the nodes where  $\text{SiO}_2$  is unaffected. The interface, which represents the reaction front, is a single node, which is in Regime 1 and where the quantity of  $\text{SiO}_2$  is decreasing with time. Nodes further in the interior are in Regime 1 and have the starting composition, while nodes nearer the surface are in Regime 2 and are exhausted of  $\text{SiO}_2$ .

The movement of the reaction front from the surface of the sample to the center is clearly shown. When the reaction front reaches the center,  $\text{SiO}_2$  is completely exhausted at all the nodes and this corresponds to the time for complete  $\text{SiO}_2$  removal, or  $t_c$ . For the “standard” case,  $t_c = 3060$  s (Table II). The behavior of the C concentration is the same except that there is some residual carbon, because a small excess is included in the starting composition to ensure complete removal of  $\text{SiO}_2$ . This will be discussed in more detail later, but approximately 3 moles of C are needed to remove each mole of  $\text{SiO}_2$ .

#### IV. Results and Discussion

The model has been used to investigate the effect of the various parameters on the time needed for complete  $\text{SiO}_2$  removal. These studies involve holding all parameters the same as in

the “standard” case defined in Table II except for the parameter of interest.

##### (I) Porosity

The effect of porosity  $\epsilon$  on the holding time needed for complete  $\text{SiO}_2$  removal is shown in Fig. 5(a), using “standard” parameter values except that porosity is varied. It should again be mentioned that an open porosity is assumed in this work.

As expected, the holding time is found to increase with decreasing sample porosity. Clearly, one reason for this is that a lower porosity impedes diffusion. A second reason is that samples of higher density but fixed composition contain more  $\text{SiO}_2$ ; therefore, more CO must be removed to completely deplete the  $\text{SiO}_2$ . The amount of CO to be removed is proportional to the amount of  $\text{SiO}_2$  which itself is proportional to  $(1-\epsilon)$ . Equation (8) shows that the diffusion coefficients are proportional to  $\epsilon$ , so that the time for complete removal is expected to be proportional to  $\epsilon^{-1}$ . Combining these two effects suggests that the time for complete removal should depend linearly on  $(1-\epsilon)/\epsilon$ . Figure 5(b) verifies this relationship.

It is noted that the pore size is held constant for these calculations, meaning that changing the porosity is changing the number of pores, but not their size. For a particular starting powder, this will not be the case—the number of pores will be

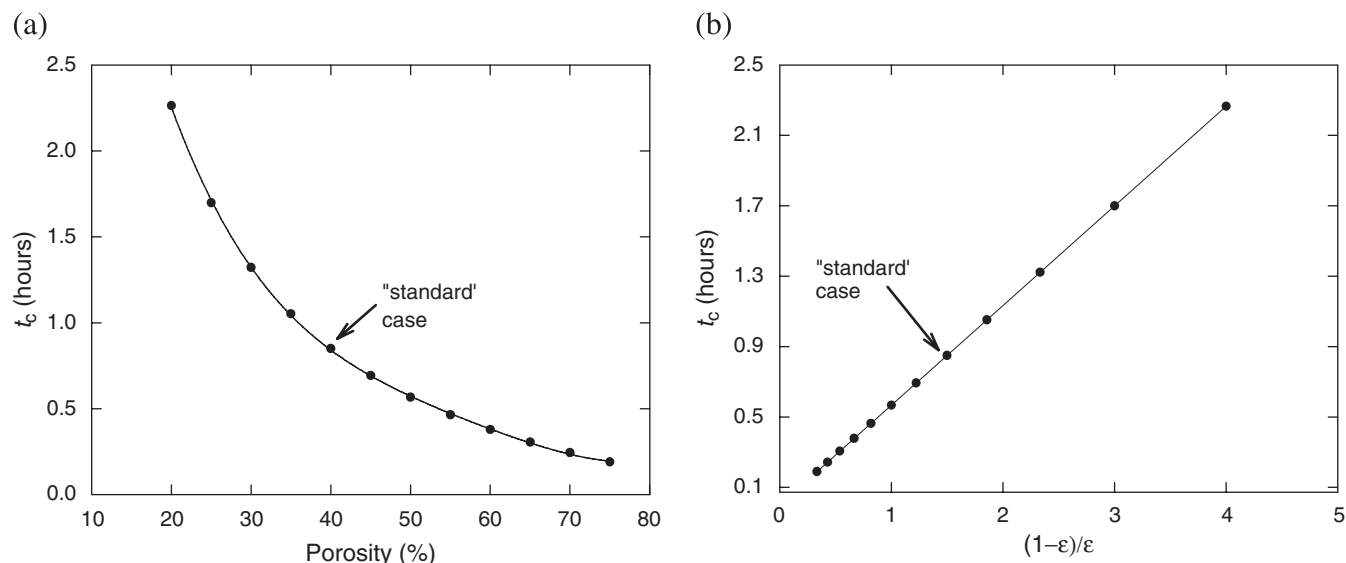


Fig. 5. Holding time for complete  $\text{SiO}_2$  removal as function of (a) porosity,  $\epsilon$  and (b)  $(1-\epsilon)/\epsilon$ .

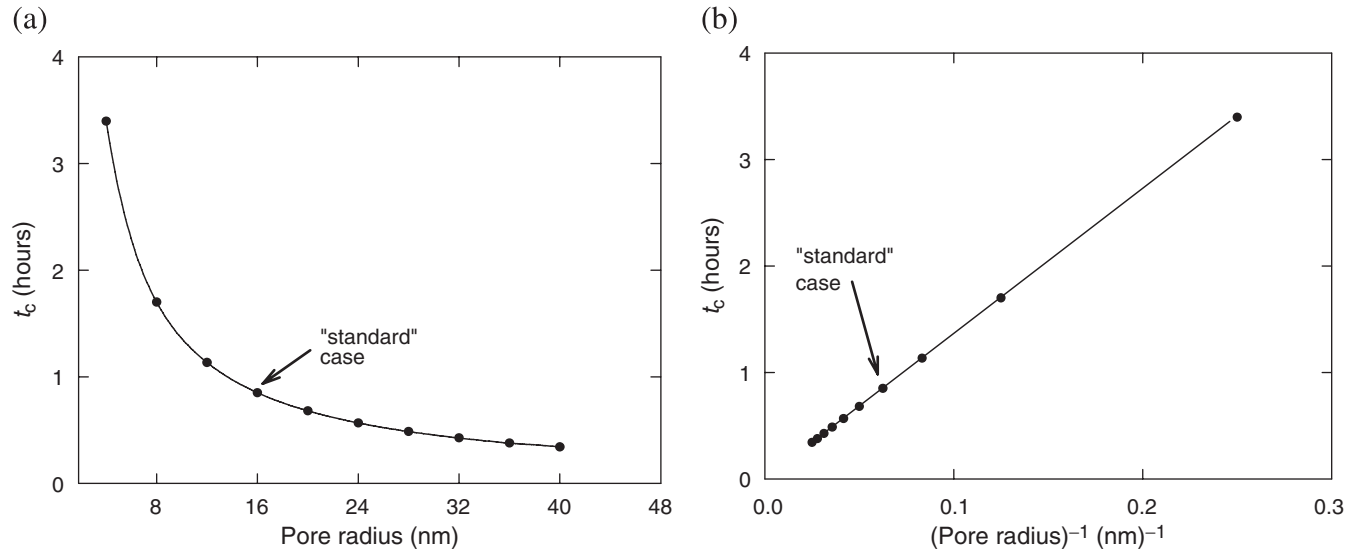


Fig. 6. Holding time required for the removal of  $\text{SiO}_2$ , as a function of pore radius on (a) a linear scale and (b) a reciprocal scale.

roughly constant with porosity, but the size of each pore will decrease with increasing density, or compaction.

## (2) Pore Size

Figure 6 shows the effect of pore size (radius)  $r$  on the holding time required for  $\text{SiO}_2$  removal at 1640 K. The pore radius is incorporated in the DGM in two places, in  $K_0$  and  $B_0$ , which have linear and quadratic dependencies, respectively (Eq. (9)). The inverse linear relationship between pore radius and holding time demonstrated in Fig. 6(b) shows that diffusion is dependent on the pore radius primarily via  $K_0$  (Eq. (7)) and the term  $B_0$  in Eq. (6) is comparatively small.

## (3) Coupling between Particle Size, Porosity, and Pore Size

For a powder with a given particle size, the pore geometry will change as the density (porosity) is changed due to pressing, or sintering. The DGM models the porosity as cylinders of radius  $r$ . In a real microstructure there will be large pores connected by narrow channels—it is these channels that the DGM considers. The overall porosity will be primarily dependent on the size and number of the large pores, while the gas diffusion will be dominated by the narrow channels. Therefore, the relationship between porosity and  $r$  will be complex and probably not predictable *a priori*. Similarly, the relationship between particle size and  $r$  will be complex. For any given system, the relationship between porosity,  $\epsilon$ , and effective cylindrical pore radius,  $r$ , would need to be determined experimentally.

## (4) Tortuosity

The tortuosity,  $q$ , of a porous body is defined as the distance between two points following a path through pores divided by the straight-line distance between the same points. It has a minimum value of one for straight cylindrically shaped pores. The pore tortuosity describes the pore structure because greater tortuosity reflects a more complex pore network. Figure 7 shows the holding time as a function of pore tortuosity. As expected, the holding time increases with tortuosity, and the linear relationship observed arises simply because of the inverse relationship between the diffusion coefficients and  $q$  shown in Eq. (8). Because the porosity  $\epsilon$  only appears in the DGM in ratio to  $q$ , it might be thought that  $(\epsilon/q)$  could be treated as a single compound variable. However, as discussed above, the overall dependence on porosity is more complex, hence the need to consider  $q$  separately.

## (5) Effect of Sample Thickness

Figure 8 shows the holding time required at 1640 K for the complete removal of  $\text{SiO}_2$  from specimens having various thicknesses,  $l$ . It can be seen that the holding time increases linearly with square of the thickness,  $l^2$ , as would be expected from simple diffusion theory. Thicker specimens contain more  $\text{SiO}_2$  to be removed as CO gas plus the diffusion path is longer, making the holding time a relatively sensitive function of the thickness.

## (6) Effect of Initial $\text{SiO}_2$ Content

It is known that the presence of  $\text{SiO}_2$  in a SiC sample is detrimental to the densification process. The main reason is the occurrence of nondensifying mechanisms, which become significant when  $\text{SiO}_2$  is present.<sup>2,3,7</sup> Modeling the influence of these mechanisms on density will be discussed in a subsequent paper. The results presented here show that the depletion of  $\text{SiO}_2$  begins near the surface and ends at the center. Hence, in the absence of proper hold times, the interior region of a SiC sample is more likely to contain  $\text{SiO}_2$  than the region near the surface. It is therefore suggested that density gradients could arise due to nonuniform removal of  $\text{SiO}_2$ , with regions near the surface exhibiting higher densities. Ness and Rafaniello<sup>7</sup> observed the appearance of density gradients in SiC samples during their work and one of the reasons attributed to this behavior was the more rapid removal of CO near the surface leading to faster reaction of  $\text{C} + \text{SiO}_2$  and hence removal of  $\text{SiO}_2$  first near the surface.

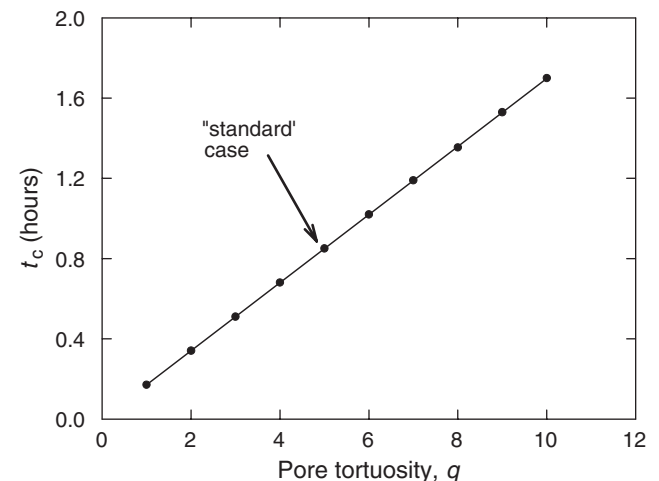


Fig. 7. Holding time required for the removal of  $\text{SiO}_2$ , as a function of pore tortuosity.

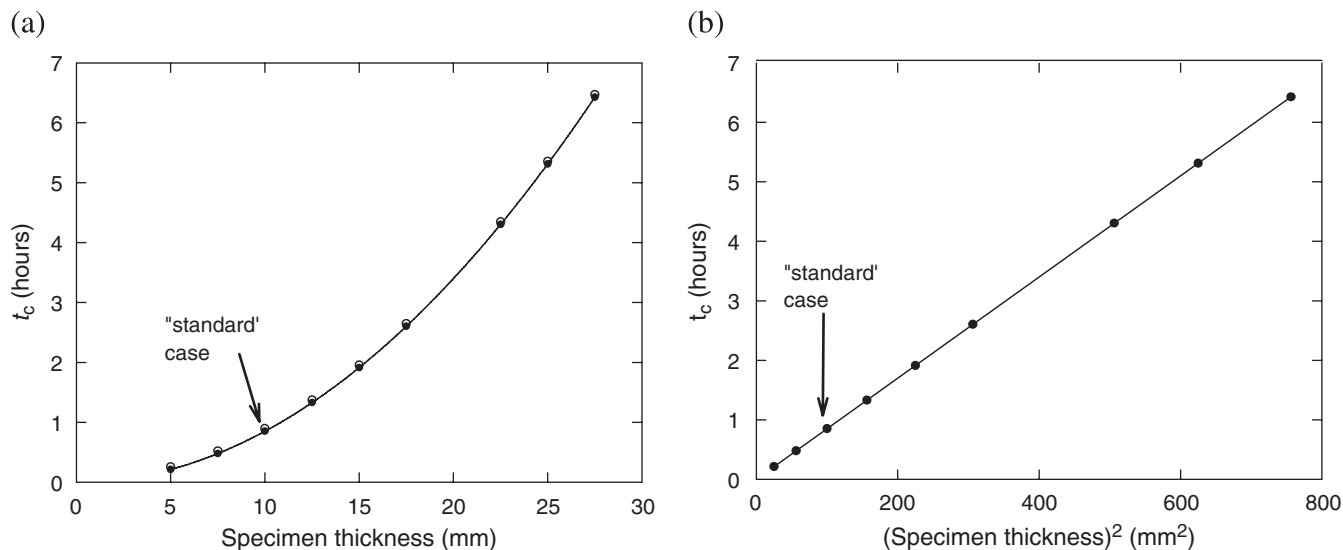


Fig. 8. Holding time required for the removal of  $\text{SiO}_2$ , as a function of (a) specimen thickness and (b) the square of the specimen thickness.

Clearly, it is advantageous to remove  $\text{SiO}_2$  before sintering. The holding time for  $\text{SiO}_2$  removal from  $\text{SiC}$  depends on the starting  $\text{SiO}_2$  content. In this work, the amount of carbon was adjusted in proportion to the amount of  $\text{SiO}_2$  with a starting  $\text{C}/\text{SiO}_2$  ratio of 3.3, which is enough to ensure complete  $\text{SiO}_2$  removal throughout the body. Figure 9 shows the holding time as a function of the mole fraction of  $\text{SiO}_2$  in the powder at 1640 K. Not surprisingly, the holding time increases linearly with the  $\text{SiO}_2$  content.

#### (7) Effect of Initial C Content

The primary reaction between C and  $\text{SiO}_2$  (rearranging Eq. (12)) is



showing that approximately three moles of C are required to remove each mole of  $\text{SiO}_2$ . Other reactions are also occurring simultaneously in the system and other gas species such as  $\text{SiO}$ ,  $\text{CO}_2$ , and  $\text{O}_2$ , are transporting small quantities of oxygen out of the system. However, under standard conditions, Eq. (13) supplies enough C, so the necessary  $\text{C}/\text{SiO}_2$  ratio is slightly less than three for the standard case defined in Table II.

This is evident from the profile of the number of moles of C remaining as a function of position at different times during the hold (under standard conditions, Table II), as shown in Fig. 4(b). Figure 10(a) is the residual C profile as a function of

position; it shows a small position-dependent quantity of C remaining at the end of the hold, due to the excess C added. Figure 10(b) shows the change in  $\text{C}/\text{SiO}_2$  ratio after depletion, further demonstrating that the required amount of C is different near the specimen surface and the interior. More C is consumed near the surface than at the interior. The amount of needed C differs from the coefficient of 3 in Eq. (34) because of the small effect of  $\text{SiO}$  diffusion. Slightly more C is needed at the surface because the  $\text{SiO}$  diffusing out from the interior reacts with the remaining carbon near the surface. The region of excess C describes a possible C distribution profile necessary for reducing the final C content in a sintering specimen.

The  $\text{C}/\text{SiO}_2$  ratio is determined for a uniform starting composition. In practice, any variability in composition will mean even more carbon needs to be added, so there is enough locally for complete  $\text{SiO}_2$  removal throughout the specimen. Local composition fluctuations below some length scale might be smoothed out by gas-phase transport and this is a topic we are currently investigating.

#### (8) Temperature

Figure 11(a) shows the variation of time for complete  $\text{SiO}_2$  removal as a function of temperature. As expected,  $t_c$  is sensitive to the temperature and is shorter at higher temperatures. The behavior is approximately linear on a semi-log plot as shown in Fig. 11(b). An Arrhenius plot ( $\ln t_c$  vs.  $1/T$ ) is also roughly linear, but the exponential dependence in Fig. 11(b) gives a better approximation to model predictions. The DGM contains temperature as  $T^{-1/2}$  through both  $D$  and  $\eta$  in Eqs. (8) and (10) respectively, and also through the equilibrium gas pressures which have an approximately Arrhenius temperature dependence via the equilibrium constants (which arises from the approximately linear temperature dependence of free energy).

The hold time can be reduced by using a higher hold temperature. If the hold time were the only consideration, the issue of  $\text{SiO}_2$  would be quite trivial. However, as will be discussed in section III(10), increasing the temperature increases the pressure of  $\text{SiO}$ , which enhances interparticle neck growth and so impedes later densification. The hold temperature should be chosen judiciously in order to minimize neck growth while still maintaining reasonably short hold times. While this issue is not examined in detail here, it will be the subject of a future publication.

#### (9) Semi Empirical Equation for the Holding Time

The dependence of holding time on an individual parameter such as sample thickness, pore size, porosity etc. is described

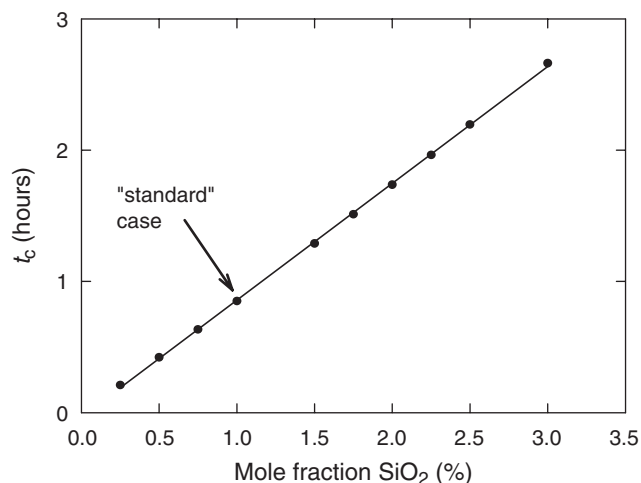
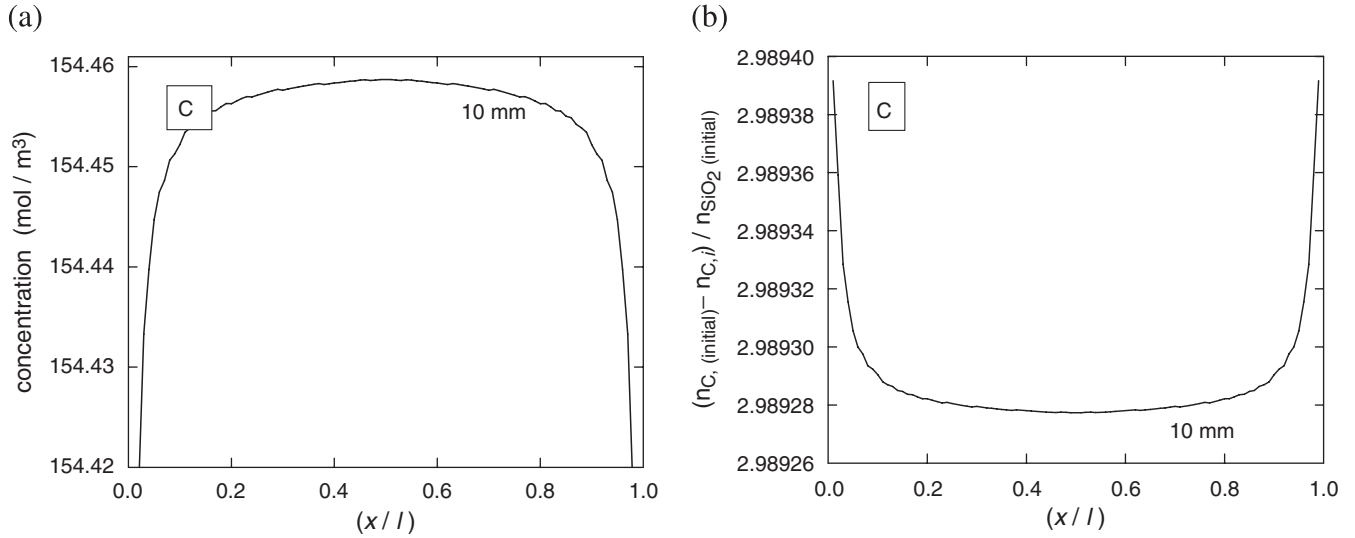


Fig. 9. Holding time as a function of initial  $\text{SiO}_2$  content in  $\text{SiC}$  powder.



**Fig. 10.** Residual C content profile after complete SiO<sub>2</sub> depletion from specimen, (a) C concentration (b) change in the number of moles of C normalized to the initial number of moles of SiO<sub>2</sub>.

earlier. In all cases, the dependence of  $t_c$  on each parameter could be put in a linearized form if a suitable function of the parameter were chosen. For example, for the dependence on porosity,  $t_c$  is proportional to  $(1-\varepsilon)/\varepsilon$ . For convenience the linearized form of  $t_c$  has been expressed centered on its value under the standard conditions given in Table III,  $t_0$ . Again using the example of porosity, this results in an equation of the form  $t_0(1 + b_\varepsilon \Delta[(1-\varepsilon)/\varepsilon])$  where  $\Delta[(1-\varepsilon)/\varepsilon]$  is the difference between  $(1-\varepsilon)/\varepsilon$  and  $(1-\varepsilon_0)/\varepsilon_0$ . The coefficient  $b_\varepsilon$  describes the sensitivity to the parameter. Table III shows these linearized forms for all the parameters under consideration, together with their coefficients.

Assuming that the dependencies of  $t_c$  on the various parameters are weakly coupled, the dependence of  $t_c$  when multiple parameters are varied simultaneously can be described by combining the equations given in Table III:

$$t_c = t_0 \left( 1 + b_\varepsilon \Delta \left[ \frac{1-\varepsilon}{\varepsilon} \right] \right) \cdot \left( 1 + b_r \Delta \left[ \frac{1}{r} \right] \right) \cdot (1 + b_q \Delta[q]) \\ \times (1 + b_l \Delta[l^2]) \cdot (1 + b_{X_{\text{SiO}_2}} \Delta[X_{\text{SiO}_2}]) \exp(-b_T \Delta[T]) \quad (35)$$

To determine whether this equation predicts results similar to those acquired by actually running the model when multiple parameters are adjusted, each parameter has been changed so

that  $t_c$  is halved, i.e.  $t_c = 0.5t_0$ . Table IV shows the adjusted values. The amount by which each parameter is varied gives an idea of how sensitive  $t_c$  is to that parameter. The model has been run for the case where all parameters are simultaneously adjusted by the amounts shown in Table IV. Under these circumstances, Eq. (35) predicts that  $t_c$  would be reduced to  $t_0/64 = 46.8$  s; the model gives a value of 48 s. This shows that the coupling between the individual parameters is weak, so that Eq. (35) makes good predictions of  $t_c$  even when the parameters are changed by a large amount. Equation (35) can therefore be used to provide guidance for the needed holding time, even for conditions where the parameters deviate significantly from the values in Table II, thus obviating the need to run the computer model for every set of experimental parameters.

#### (10) Influence of Gas Pressure on Densification

Necking is a significant mechanism that acts to decrease final density.<sup>20</sup> Three mechanisms that drive necking include vapor transport diffusion, surface diffusion and lattice diffusion. While all three mechanisms are temperature driven, vapor transport is also governed by  $p_{\text{SiO}}$  over time. Figure 12 shows the integrated SiO pressure over time, as a function of position. It is highest at the specimen center, implying greater necking and explaining observed density gradients.<sup>7</sup> If the only concern were minimizing the hold time for complete SiO<sub>2</sub> removal, then the temperature

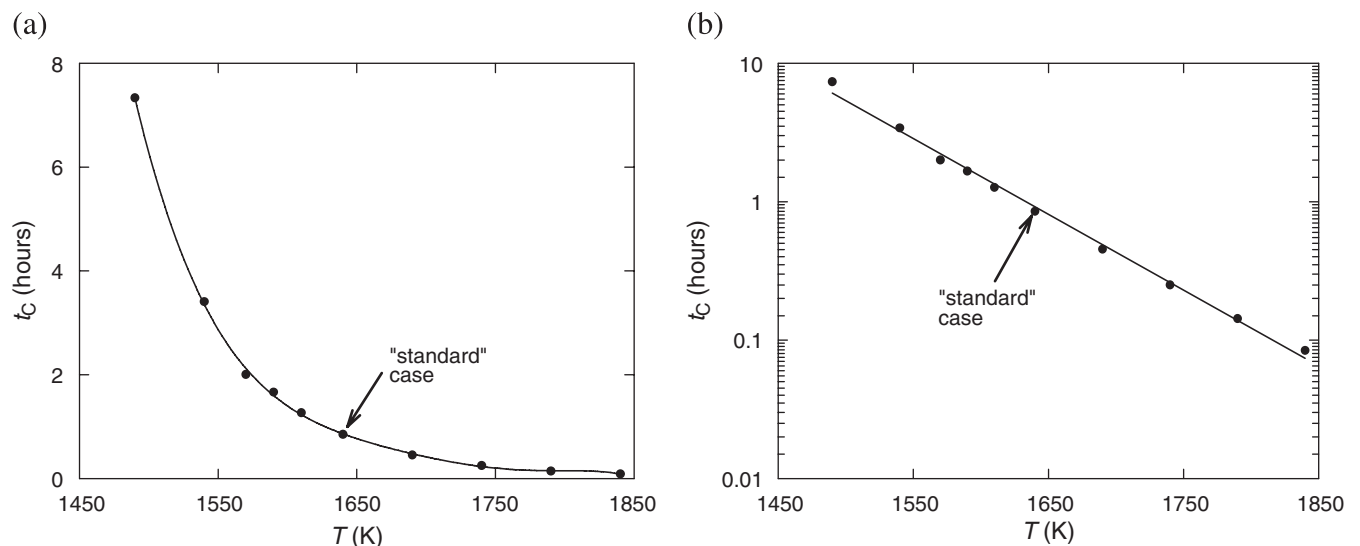


**Fig. 11.** Holding time required for the removal of SiO<sub>2</sub>, as a function of temperature on (a) linear and (b) semilog scales.

**Table III. Linearized Equations Relating Time for Complete SiO<sub>2</sub> Removal,  $t_c$ , to Each Parameter**

Parameter	Expression for $t_c$	$b_i$
Porosity ( $\epsilon$ )	$t_0(1+b_\epsilon\Delta[(1-\epsilon)/\epsilon])$	0.668
Pore radius ( $r$ )	$t_0(1+b_r\Delta[1/r])$	15.0 nm
Tortuosity ( $q$ )	$t_0(1+b_q\Delta[q])$	0.195
Specimen thickness ( $l$ )	$t_0(1+b_l\Delta[l^2])$	0.01 mm <sup>-2</sup>
Mole fraction ( $X$ )	$t_0(1+b_{X_{SiO_2}}\Delta[X_{SiO_2}])$	1.071
Temperature ( $T$ )	$t_0\exp(-b_T\Delta[T])$	0.013 K <sup>-1</sup>

$t_c$ , takes a value of  $t_0 = 0.85$  h for the standard conditions listed in Table II.

**Table IV. Semiempirical Equation Sensitivity Test**

Parameter	Reference value	0.8 $t_0$	0.5 $t_0$	0.25 $t_0$
Specimen thickness ( $l$ ) (mm)	10	8.94	7.07	5
Pore radius ( $r$ ) (nm)	16	20.3	34	80
Porosity ( $\epsilon$ )	0.4	0.454	0.571	0.726
Tortuosity ( $q$ )	5	3.97	2.44	1.15
Mole fraction of SiO <sub>2</sub> ( $X_{SiO_2}$ ) (%)	1	0.813	0.533	0.299
Temperature ( $T$ ) (K)	1640	1657.2	1693.3	1746.6
Actual $t_c$ (s)	3060	801.9	47.8	0.189
Calculated $t_c$ (s)	3060	802.2	46.8	0.747

could be maximized. However, this increases the SiO partial pressure so that the neck growth is enhanced, even though the time for that neck growth is decreased. Therefore choice of the hold temperature is a balance between reducing the hold time without unduly increasing the neck growth. This phenomenon will be examined in more detail in a subsequent paper.

## V. Conclusions

A computational model describing the kinetics of multi species gas diffusion during the initial stages of sintering of SiC has been developed, assuming reaction kinetics are fast, so that locally, thermodynamic equilibrium is maintained (this assumption is justified since density gradients are observed in bodies of size  $\sim 1$  cm which would not be the case were reaction kinetics rate controlling). The so-called DGM is used to describe the diffusion and is valid for pore sizes significantly larger than the size of the

gas molecules, which is the case for typical SiC green bodies. The model enables prediction of the needed intermediate holding time for complete removal of SiO<sub>2</sub> by gas-phase diffusion. The dependence of this holding time on various parameters, such as temperature, etc., has been studied. The model can be used to help determine an efficient heating cycle for the fabrication of dense SiC components.

The quantities of solid and gas species were monitored as a function of time and position across the sample thickness. It was found that a reaction front travels from the surface of the sample toward the center with SiO<sub>2</sub> exhaustion taking place at the reaction front. The time required for complete removal of SiO<sub>2</sub> therefore corresponds to the time taken for the reaction front to reach the center of the specimen. A semiempirical equation has been developed to describe how the holding time varies with all the influencing parameters. This equation was found to represent the model well even when several parameters are varied simultaneously.

The model confirms that the kinetics of SiO<sub>2</sub> removal is controlled by the rate of diffusion of CO, because all other gas species are at significantly lower pressure as was suggested by Ness and Rafaniello.<sup>7</sup> The results are qualitatively consistent with published experimental results showing gradients in properties from the surface to the interior. There are very few data in the literature that can be used to validate the model in more detail. However, because the model is based on well-known gas kinetic theory, its predictions will be qualitatively correct. Therefore the model does provide useful guidance for how the heating cycle can be optimized while minimizing the amount of experimentation needed.

A model of this sophistication forms the basis for much work that is currently in process and to be published in future papers. The inclusion of a number of minor gases is dictated by future research needs. For instance, SiO pressure is a key parameter in SiC interparticle neck growth; its inclusion allows the examination of this phenomenon. (Note that controlling the SiO pressure limits the hold temperature—the hold time cannot be minimized simply by increasing the temperature.) The influence of ambient atmosphere and inert gas will be examined, thus justifying the use of a full multiple species implementation of the DGM. Finally, the model allows for the examination of other material systems, such as B<sub>4</sub>C, including those that do not involve a single dominant gas such as CO.

## References

1. Prochazka, "Sintered Dense Silicon Carbide"; NY United States. Pat. No. 4004934, 1977.
2. W. Rijswijk and D. J. Shanefield, "Effects of Carbon as a Sintering Aid in Silicon Carbide," *J. Am. Ceram. Soc.*, **73** [1] 148–9 (1990).
3. W. J. Clegg, "Role of Carbon in the Sintering of Boron-Doped Silicon Carbide," *J. Am. Ceram. Soc.*, **83** [5] 1039–43 (2000).
4. S. Prochazka and R. M. Scanlan, "Effect of Boron and Carbon on Sintering of SiC," *J. Am. Ceram. Soc.*, **58** [1] 72 (1975).
5. M. Raczka, G. Gorney, L. Stobierski, and K. Rozniatowski, "Effect of Carbon Content on the Microstructure and Properties of Silicon Carbide-Based Sinters," *Mater. Charact.*, **46**, 245–9 (2001).
6. L. Stobierski and A. Gubernal, "Sintering of Silicon Carbide: I. Effect of Carbon," *Ceram. Int.*, **29**, 287–92 (2003).
7. E. A. Ness and W. Rafaniello, "Origin of Density Gradients in Sintered B-Silicon Carbide Parts," *J. Am. Ceram. Soc.*, **77** [11] 2879–84 (1994).
8. R. Hamminger, "Carbon Inclusions in Sintered Silicon Carbide," *J. Am. Ceram. Soc.*, **72** [9] 1741–4 (1989).
9. R. M. German, *Sintering Theory and Practice*, pp. 115–21. John Wiley & Sons Inc., New York, 1996.
10. E. A. Mason and A. P. Malinauskas, *Gas Transport in Porous Media; the Dusty-Gas Model*. Elsevier, Amsterdam, the Netherlands, 1983.
11. J. O. Hirschfelder, C. F. Curtiss, and R. B. Bird, "Transport Phenomena of Dilute Gases"; pp. 514–610 in *Molecular Theory of Gases and Liquids*, 1st edition, John Wiley and Sons, New York, NY, 1954.
12. W. D. Kingery and M. Berg, "Study of the Initial Stages of Sintering Solids by Viscous Flow, Evaporation-Condensation, and Self-Diffusion," *J. Appl. Phys.*, **26**, 1205–12 (1955).
13. G. W. C. Kaye and T. H. Laby, *Tables of Physical and Chemical Constants*, 16th edition, Longman, Harlow, U.K., 1995.
14. S. H. Kang and J. A. Kunc, "Molecular Diameters in High Temperature Gases," *J. Phys. Chem.*, **95**, 6971–3 (1991).

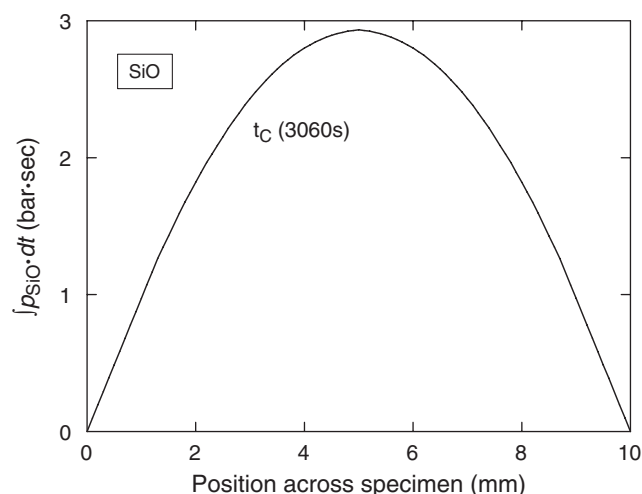


**Fig. 12.** Cumulative partial pressure of SiO over time (to SiO<sub>2</sub> exhaustion at  $t_c = 3060$  s), as a function of position through the specimen thickness.

<sup>15</sup>E.S. Microware Inc. *TAPP 2.2, Version 2.2*. E.S. Microware Inc., Wade Court, Hamilton, OH.

<sup>16</sup>M. W. Chase, D. C. Washington, *JANAF Thermochemical Tables*, 3rd edition, Vol. 1–2. American Institute of Physics, New York, 1986.

<sup>17</sup>J. D. Cox, D. D. Wagman, and V. A. Medvedev, *CODATA Key Values for Thermodynamics, Final Report of the CODATA Task Group on Key Values for Thermodynamics*. Hemisphere Pub. Corp., New York, 1989.

<sup>18</sup>National Institute of Standards and Technology. *NIST Chemistry WebBook*. National Institute of Standards and Technology, Gaithersburg, MD. Available at <http://webbook.nist.gov/>, 2005.

<sup>19</sup>A. Kaza, “Effect of Gas Phase Composition in Pores During Densification; Ph.D. dissertation, Rutgers University, Piscataway, NJ, September 2006.

<sup>20</sup>Y. M. Chiang, D. III Birnie, and W. D. Kingery, *Physical Ceramics, Principles for Ceramic Science and Engineering*, pp. 398–404. John Wiley & Sons, Inc., New York, 1997. □